QUANTIFYING THE HEAT TRANSFER EFFECT OF THE AXIAL TURBINE STATOR WELL CAVITY

Qun YAN[1], Peng SUN[1] *, Qinqin MU[1], Yonghui CHEN[1]

[*1]National Key Laboratory of Strength and Structural Integrity, Aircraft Strength Research Institute of China, Xi'an 710065, China

[*] Corresponding author; E-mail: sunp065@avic.com

A Thermal-Fluid-Structural model is presented for quantifying the heat generation by the labyrinth seal in the low-pressure turbine stator well cavity. The method combines windage heating and convective heat transfer effects for labyrinth seal design, making it possible to use the heat transfer boundary condition instead of adiabatic to do the computational fluid dynamic calculation. The solutions illustrate how the outlet total temperature may change depending on the seal pressure ratios, windage heating, and heat transfer coefficient. It is further demonstrated that with a fixed seal pressure ratio, the thermal boundary condition has little influence on the leakage flow rate of the seal. The total temperature rise is dependent on the thermal boundary conditions, including the stator/rotor wall temperature, heat transfer coefficient, and windage heat caused by air friction.

Key words*: labyrinth seal, aero-engine, turbine stator well, heat transfer, windage heating, numerical simulation, leakage flow rate*

1. Introduction

The leakage behaviors and thermal features of labyrinth seals are the major focus of research. Thermal feature research focuses on fluid and rotor/stator heat transfer, as well as total temperature rises due to windage heating. Micio et al. [1] found that pressure difference, Reynolds number, and seal radial clearance all had an impact on sealing effectiveness, and the experimental findings revealed that clearance had a significant impact on leakage loss, heat transfer, and the evolution of flow fields. He et al. [2] used the conjugate heat transfer method to analyze windage heating in stepped labyrinth seals, and the distributions of heat transfer coefficients for rotors and stators with various configurations were studied in depth. The existence of rub-grooves in honeycomb land and their influence on seal performance were examined by Charan Nayak et al. [3]. Rub-grooves caused greater seal leakage and reduced windage heating. The rise in windage heating coefficient was virtually linearly related to the rotating speed, according to Kong et al. [4], and increasing the radial clearance resulted in a decrease in windage heating coefficient. Michael Flouros et al. [5] carried out the CFD analysis on the windback seal, which could prevent oil migration out of the oil chamber. To examine the flow properties of the labyrinth seal, Campagnoli et al. [6] developed a 1-dimensional hydraulic network and a 2-dimensional thermal framework with an iterative loop structure. Sun et al. [7] utilized numerical modeling and practical testing to evaluate the flow characteristics and effect of windage heating for labyrinth seals with different heights of teeth, which rose with increasing rotational

velocity and reduced with rising pressure difference. Based on their prior study, Charan Nayak et al. [8] studied the rotation impact on leakage of the seal and the windage heating effect of the seal. The seal discharge coefficient stayed constant as the angular velocity rose until a critical speed of rotation was attained. The impact of changing geometric parameters on the heat transfer and leakage properties of labyrinth seals at different rotational speeds was examined by Wang et al [9]. Shi et al. [10] proposed the nonuniformity coefficient to assess the effect of nonuniform clearance on windage heating and the development of swirls in straight-through labyrinth seals. Zhang et al. [11] investigated the relationship between seal leakage and heat transfer under different pressure ratios using the experimental orthogonal method. Yang et al. [12] used numerical simulation to evaluate the sealing capacity and heat transfer properties of a straight-through labyrinth seal with varying geometric parameters (gap width, tooth tip thickness, and front inclination angle). Sun et al. [13] investigated the mutual influence of the buffer air seal and the oil seal in the support seal system using the CFD-FEA loosely coupled approach. Shi et al. [14] utilized conjugate heat transfer (CHT) analysis and structural finite element method (FEM) analysis to evaluate the elastic deformation, leakage flow, and heat transfer of the labyrinth seal. Jackson et al. [15] indicated the results of a collaborative experimental and numerical campaign to investigate the relationship between windage torque and flow physics in a scaled low-pressure turbine stator-well design.

A common assumption often made of labyrinth seal research by previous re-searchers is that they are considered adiabatic; however, due to the flow passing through the narrow seal clearance, heat transfer different from windage heating could not be ignored. This research investigation combined the use of computational simulations and a thermal fluid analysis model to take a deeper look into the heat generation within a low-pressure turbine stator well, which could be useful to guide the mechanical design of the seal ring. For the purpose of defining the nomenclature and il-lustrating the fundamental flow patterns, Figure 1 depicts a typical turbine stator well.

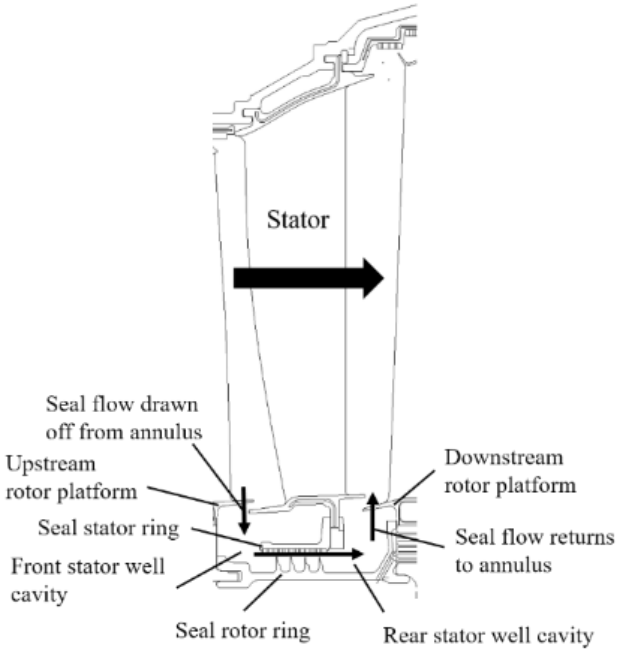

Figure 1. Terminology and basic flow directions in a turbine stator well

Computational simulations were used to further investigate the effect of heat transfer via the turbine stator well, which showed the importance of incorporating convective heat transfer into the

model and applying the correct thermal boundary conditions to the boundary wall. Overall, this investigation seeks to establish the correct thermal boundary condition and approach for validation of the computational model. It also aims to quantify the impact that heat transfer has on total temperature rise and heat generation for turbine stator wells. Figure 2 demonstrates the research concept in this work, which is based on the geometry of the turbine stator well, evaluates the leakage flow rate through numerical simulation and empirical relation equations, further investigates the windage heating power in the seal region, convective heat transfer, uses the Thermal-Fluid-Structural model to determine the overall heat generation in the seal, and iteratively designs the seal structural parameters based on the heat generation that can satisfy the working requirements of the aero-engine.

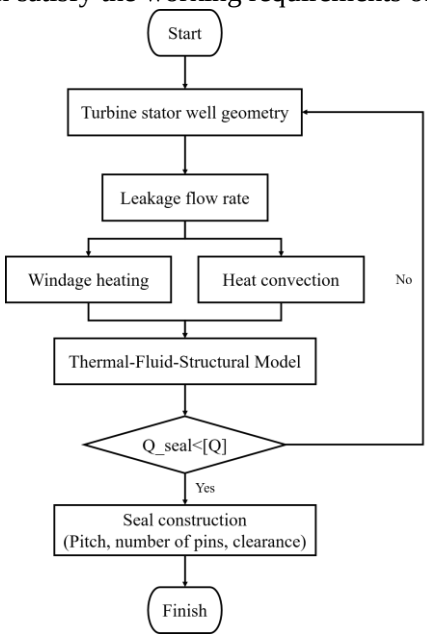

Figure 2. Design process of turbine stator well

2. Computational model

2.1. Model and Meshing

In this paper, the model of the low-pressure turbine stator well is simplified, as shown in Figure 3 and Figure 4. The leakage flow enters from the left top side of the structure and returns to the annulus main flow path from the right top side. The sealing structure is the straight-through labyrinth seal, and the typical parameters of the seal pin are given in Table 1.

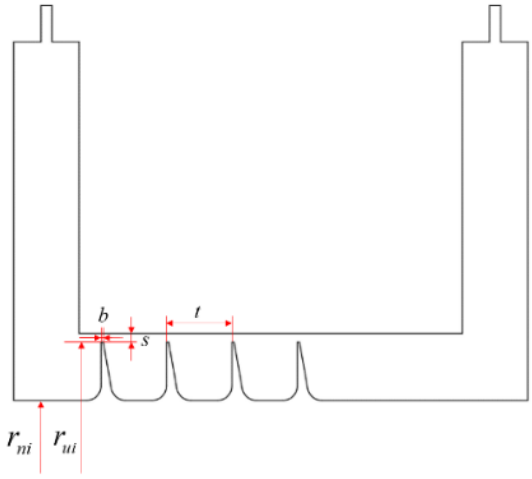

Figure 3. Scheme of the simplified low-pressure turbine stator well

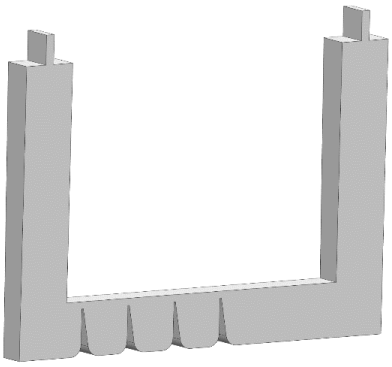

Figure 4. 3D model of the simplified low-pressure turbine stator well

Table 1. Geometrical parameter of the 4-knives labyrinth seal at the low-pressure turbine stator well

Parameter	Value	Unit
Radial clearance (s)	1.2	mm
Seal tip width (b)	0.3	mm
Seal pitch (t)	9	mm
Number of seal pins (z)	4	-
Seal tip radius (r_{ui})	281.75	mm
Rotor radius (r_{ni})	273.75	mm

The 3D seal geometry models are then meshed by using ANSYS Meshing with unstructured triangular meshes. The generation of good-quality mesh for knife tip clearance is important to capture flow features near the knife edges. Good-quality mesh can be generated in knife tip gaps by controlling its critical parameters, such as the sphere radius and element size on the knife tip, the height of the first layer and maximum layers of the non-uniform boundary layer, the growth rate in the inflation option, etc. The height of triangular elements adjacent to the outer layer of the boundary layer grid should be roughly the same as the height of elements in the outer layer of the boundary layer grid. Such node distribution is particularly important to avoid jumps in flow variable values across the interface of structured and unstructured types of grids. Figure 5 shows the details of mesh in the seal chamber and in knife tip clearance.

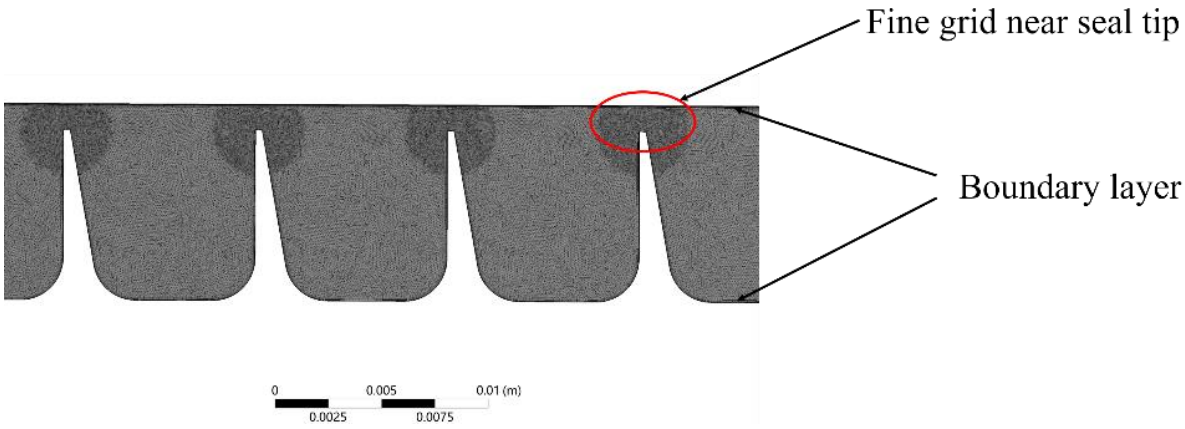

Figure 5. Mesh detail of the seal region

2.2. Boundary conditions

Detailed settings of the CFD model and boundary conditions are listed in Table 2. As shown in Figure 6, the inlet total pressure is kept constant, and the static pressure at the downstream end of the turbine stator well was prescribed to give a pressure ratio of 1.08 to 1.8. Adiabatic and non-adiabatic thermal boundary conditions are both applied in the CFD simulations. For the adiabatic wall boundary condition, it is aimed at obtaining the windage heating associated with the air friction. For the non-adiabatic wall boundary condition, it is aimed at obtaining the heat transfer coefficient (HTC) distribution along the rotor/stator surface, which is modeled as convective walls with a heat flux. According to ANSYS CFX, the heat transfer coefficient is

$$HTC = \frac{Q}{T_w - T_{ref}} \tag{1}$$

where T_w denotes the static temperature of the cell closest to the wall, T_{ref} is adopted by the inlet total temperature of the seal region. For the heat transfer coefficient, it was explicitly specified T_{ref} to generate a variable in post-processing, and then the coordinates and HTC for each cell along the seal were exported as a matrix.

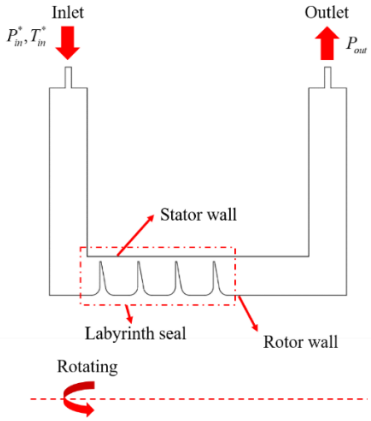

Figure 6. CFD computational domain

Table 2. Boundary conditions and CFD settings

Parameter	Value	Unit
Inlet total pressure (P_{in}^*)	200	kPa
Inlet total temperature (T_{in}^*)	673	K

Outlet static pressure (P_{out})	125	kPa
Rotating speed (N)	4703	rpm
Turbulence model	SST with automatic wall treatment	
Convergence criteria	Mass flow rate balance	
	Outlet total temperature do not change over iterations	

2.3. Grid independence validation

Before deciding the grid density for actual numerical simulation, a grid convergence study should be carried out. The variation of the leakage flow rate with the pressure ratio under the conditions of different grid numbers is calculated, and the results are shown in Figure 7. When the grid number is increased from 1.07 million to 1.7 million, the change in leakage flow rate is 0.02%, so the grid number of 1.07 million can satisfy the grid independence requirement.

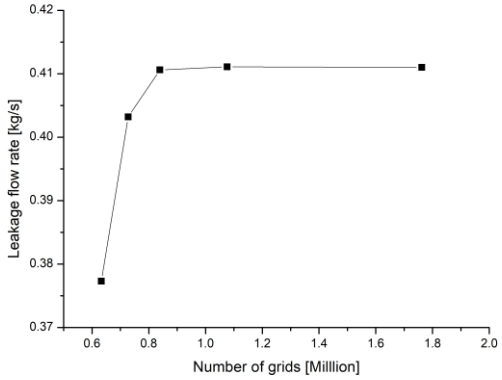

Figure 7. Grid-independent test

3. Leakage flow rate

The leakage performance of the labyrinth seal can be predicted using a variety of approaches, such as empirical formulas and CFD simulations. The initial estimation of the leakage flow rate in this investigation where the critical flow did not occur in the labyrinth passages is based on the empirical relationship shown in the following equations [16], which takes into account the relationship between the leakage flow rate and the structural parameter of the labyrinth seal.

$$G=\varphi KF\sqrt{\frac{\left(P_{in}^{*}\right)^{2}-P_{out}{}^{2}}{zRT_{in}^{*}}} \tag{2}$$

Where, G denotes the leakage flow rate; F denotes the leakage area; R denotes the gas constant; φ denotes the flow coefficient; K denotes the correction factor.

The flow coefficient of the seal depends on the rate of s/b, it can be expressed as:

$$\varphi=0.792-0.06945s/b+0.01146\left(s/b\right)^{2} \tag{3}$$

For the stepped labyrinth seal, correction factor K equals to one; for the straight-through labyrinth seal, correction factor is related to the number of pins and seal pitch, it can be expressed as:

For the case of $z\le 20$ and $s/t\le 0.13$,

$$K = a_0 + a_1 z + a_2 z^2 + a_3 z^3 \tag{4}$$

$$a_0 = 0.9555 - 3.471 s/t + 10.79 (s/t)^2 \tag{5}$$

$$a_1 = 0.1238 + 2.888 s/t - 7.238 (s/t)^2 \tag{6}$$

$$a_2 = -0.0148 - 0.1942 s/t + 0.6369 (s/t)^2 \tag{7}$$

$$a_3 = 0.00043285 + 0.005049 s/t - 0.01942 (s/t)^2 \tag{8}$$

For the case of $z > 20$, $z = 20$; for the case of $s/t > 0.13$, $s/t = 0.13$.

4. Heat generation

One of the objectives of this investigation is to establish the overall heat generated in the air flow as it enters the upstream region, passes through the labyrinth seal, and enters the downstream region. In this paper, we consider the engine operating state at which the wall temperature is assumed to be higher than the gas temperature, at which the temperature of the cooling flow through the labyrinth seal passage will increase.

In general, the heat flux along the seal region is calculated using a heat balance, as illustrated in Equation 9, with the heat flux components provided in Figure 8. The total heat transfer in the seal is partly due to frictional heat from windage heating and partly due to convective heat transfer.

$$Q_\Sigma = Q_{out} - Q_{in} = Q_{conv} + Q_{windage} = G \cdot C_p \left(T_{out}^* - T_{in}^* \right) \tag{9}$$

Where T_{in}^* and T_{out}^* are taken as the average total temperature at the inlet and the outlet, and C_p denotes the gas specific heat capacity at different temperature.

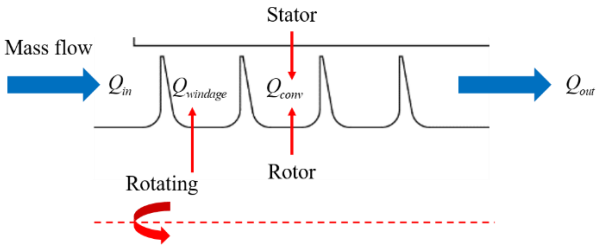

Figure 8. Heat generation along the seal

4.1. Windage heating

Millward and Robinson [17] concluded from their experimental labyrinth seal rig work that windage heating through labyrinth seals:

$$Q_{windage} = 0.5 \times 10^3 C_{ms} \rho \omega^3 r_{ui}^3 F \tag{10}$$

$$C_{ms} = 0.05993\left(\frac{G}{\rho w r_{ui}^3}\right)^{\alpha} z^{-0.65} \tag{11}$$

Where ρ denotes the gas density, ω denotes the rotating velocity and α denotes the empirical coefficient, which corresponds to the working condition of the seal.

In order to study the windage heating separately, for the CFD simulations, the boundary conditions of the seal rotor/stator walls are assumed to be adiabatic. As a result, all windage power received in a rotor/stator system should be lost as heat into the leakage flow in an adiabatic system. The total temperature rise due to internal losses and heat produced in the seals is therefore calculated as windage heating.

4.2. Heat transfer

This section describes the technique and functioning of the labyrinth seal's 1D axisymmetric heat transfer model. Figure 9 depicts a flow chart of the computation procedure. To determine heat transfer coefficients h, the CFD calculation was applied according to Section 2.2. A mean value model for total temperature rise is used to calculate the average temperature of the stator and rotor walls. A linked thermal-fluid-structural model is formed by combining the mean value model and the CFD model.

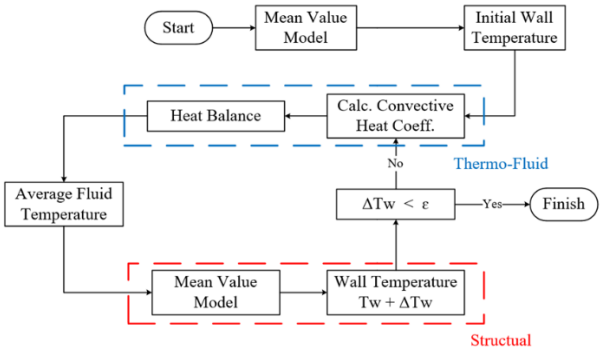

Figure 9. Flow chart of thermal-fluid-structural model and heat balance across labyrinth seal

The seal outlet gas temperatures determined by the adiabatic wall are utilized as the fluid domain's first guess. Then, an initial estimation of the mean value model of the wall temperature is utilized to calculate the rotor and stator walls first mean temperature. Using the starting wall temperature, a heat balance is used to compute convective heat fluxes between the rotor/stator surface and the cooling flow, which is illustrated in Equation 9. Convective heat fluxes are computed, and the temperatures of the seal outlet gases are updated. The average temperature of the wall is then recalculated using the heat transfer coefficients (HTC) and outlet gas temperatures. Iteratively, the method is repeated until a convergence requirement is fulfilled.

In order to simplify the thermal-fluid-structural computational model and improve computational efficiency, this work replaces the thermal conduction calculation process of the rotor or stator by using the mean value model.For the mean value model for rising temperature inside a straight-through labyrinth seal, it is based on three factors: the input total temperature, the total temperature rise of the gas, and heat transfer models. The temperature is affected by a number of operational characteristics, including leakage flow rate, radial clearance, rotating speed, and pressure differential.

A basic PDE for a one-dimensional flow is given and calculated for the outlet total temperature to describe the total temperature rise in the seal.

$$T_{out}^{*} = T_w + \left(T_{fluid} - T_w\right) e^{-\frac{hA}{GC_p}} \tag{12}$$

Where, A denotes the seal rotor outer surface area, T_w denotes the wall temperature of the rotor surface.

The gas temperature at the seal inlet will be known, and the gas temperature at the outlet will be determined using the initial CFD results with adiabatic boundary conditions. The wall temperature is assumed to be evenly distributed and Equation 13 will be used to determine the wall temperature.

$$T_w = \frac{T_{out}^{*} - T_{in}^{*} e^{\frac{-2h\pi r_{ui}L}{GC_p}}}{1 - e^{\frac{-2h\pi r_{ui}L}{GC_p}}} \tag{13}$$

A temperature mean value can be calculated with Equation 14.

$$\Delta T_{\ln} = \frac{\Delta T_2 - \Delta T_1}{\ln(\Delta T_2 - \Delta T_1)} \tag{14}$$

Where,

$$\Delta T_1 = \left|T_w - T_{out}^{*}\right| \tag{15}$$

$$\Delta T_2 = \left|T_w - T_{in}^{*}\right| \tag{16}$$

From this, the heat flow from the convection can be calculated with Equation 17, and from Equation 19, a new value of the seal outlet temperature can be determined. A new value of the wall temperature can be calculated, and the procedure is iterated until the wall temperature converges.

$$Q_{conv} = hA\Delta T_{\ln} \tag{17}$$

$$Q_{\Sigma} = Q_{conv} + Q_{windage} \tag{18}$$

$$Q_{\Sigma} = G \cdot C_p \cdot (T_{out}^{*} - T_{in}^{*}) \tag{19}$$

5. Results

5.1. Leakage flow rate

For the validation process of the given empirical model, the results of the empirical relationship were compared with the CFD calculations with adiabatic and non-adiabatic boundary conditions. All the leakage flow rates obtained were nonlinearly increasing as a function of the pressure ratio. Figure 10 summarizes the leakage performance obtained for the case with different pressure ratios. Importantly, the CFD model does not take into account the structural deformation of the seal stator and rotor parts caused by the centrifugal load and thermal expansion. Therefore, there are low leakage

flow rates with CFD calculations compared with the empirical relation-ship. But the thermal boundary conditions have little influence on the leakage flow rate.

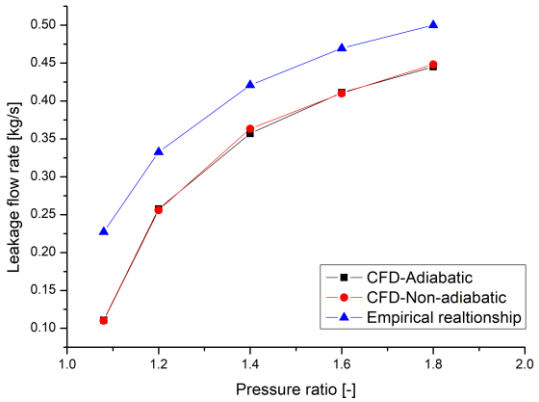

Figure 10. Leakage flow rate at the labyrinth seals for varying seal pressure ratios

5.2. Windage heating

In this section, windage heating on the cavity leakage flow for varying seal pres-sure ratios as well as the contributions of the cavity wells and labyrinth seals to the overall windage heating are presented. Figure 11 shows that windage heating in-creases with an increasing seal pressure ratio. The CFD calculation results are consistent with the results of the Millward and Robinson model, but the value is larger. For lower pressure ratios, the leakage flow through the cavity is relatively low, which results in less shear work done on the gas as opposed to larger pressure ratio cases, as well as less windage heating.

Figures 12 and 13 show the total temperature at the inlet and outlet sections of the labyrinth seal as well as the rise in total temperature. First, Figure 12 shows both incoming and outgoing leakage flow temperatures are higher for lower pressure ratios. More importantly, as the seal pressure ratio increases, the seal outlet temperatures reach an almost asymptotic value because increased flow rates at larger pressure ratios make momentum transfer more difficult, resulting in lower temperatures. Therefore, higher pressure ratio cases, which are a criterion for improved aerodynamic performance of the low-pressure turbine, will have higher cavity well temperatures as a result of less cavity leakage flow through the seal. Then, the interdependence of total temperature rise and pressure ratio is shown in Figure 13. The plot shows that lower seal pressure ratios achieve a higher increase in total temperature rise. Therefore, investigating pressure development along the seal is crucial for understanding the development of temperature in the cavity wells.

Additionally, Figure 14 shows the windage heating contributions by the front and rear wells and labyrinth seals. In all cases, at least 35 percent of the windage work is generated in the front cavity well, approximately 30 percent by the labyrinth seals, and approximately 35 percent by the rear cavity well. In all the cases of 1.08 to 1.80 span pressure ratios, the front and rear cavity wells tend to show increasing contributions to windage heating.

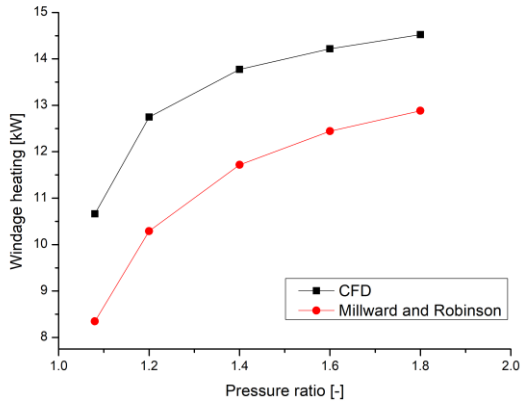

Figure 11. Changes in windage heating at the labyrinth seals for varying seal pressure ratios

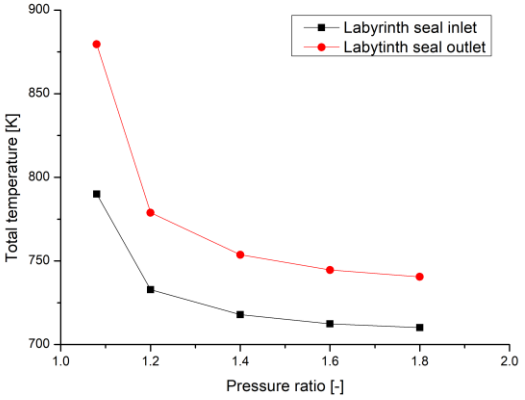

Figure 12. Changes in total temperature at the labyrinth seals inlet and outlet for varying seal pressure ratios

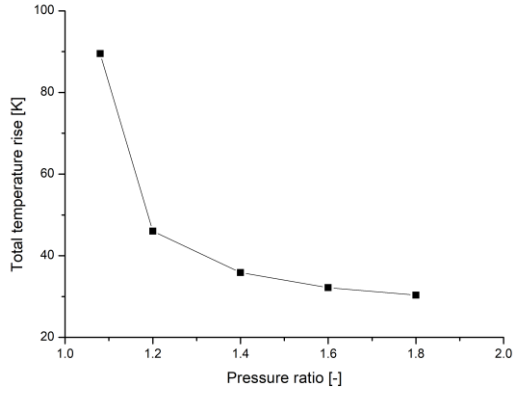

Figure 13. Changes in total temperature rise at the labyrinth seals for varying seal pressure ratios

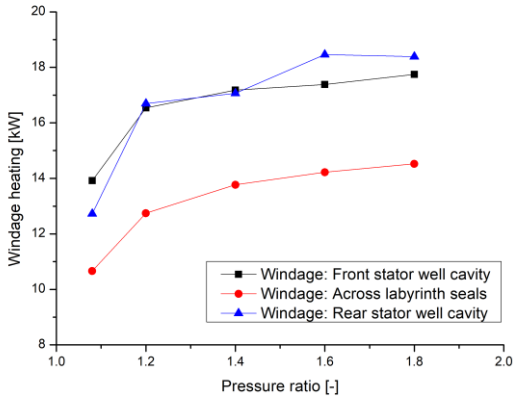

Figure 14. Windage heating contributions by the cavity for varying seal pressure ratios

5.3. Total temperature rise

CFD calculations with adiabatic surface boundary condition has been executed to get the windage heating, and the heat flow from the convection has also been integrated into the thermal-fluid-structural model. In order to study the heat transfer effect along the seal, the current work acquired the HTC distribution along the seal rotor/stator in the low-pressure turbine stator well based on the CFD calculations in Section 2, which is helpful to investigate the heat transfer effect in the seal region. The numerical simulations use a 1° section of the turbine stator well to account for the rotating effect. The boundary conditions are retained from Table 2, as are the geometry parameters from Figure 3 and Table 2. A 5000 W heat flux property is defined on the surface of the seal rotor and stator.

Figure 15 plots the distributions of the heat transfer coefficient along the axial direction for the seal rotor surface in the situations of (N = 4703 rpm, s = 1.2 mm, Pressure ratio = 1.6). It is obvious that from the labyrinth seals inlet to outlet, the heat transfer coefficient decreases. Figure 16 shows the distributions of the heat transfer coefficient for the seal stator surface at (N = 4703 rpm, s = 1.2mm, Pressure ratio = 1.6) in the axial direction. As can be observed, the heat transfer coefficient also decreases along the axial direction. Then, we could obtain the average heat transfer coefficient along the seal rotor/stator.

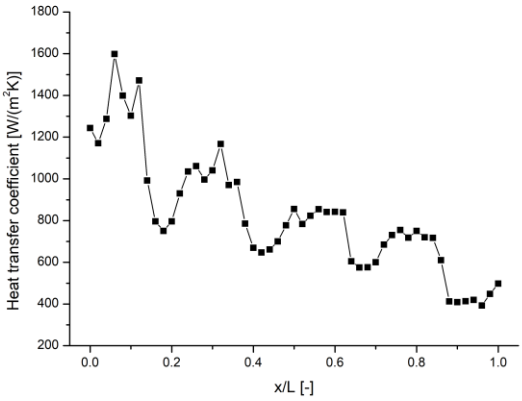

Figure 15. HTC distributions for the rotor surface (Pressure ratio = 1.6, N = 4703 rpm, s = 1.2 mm)

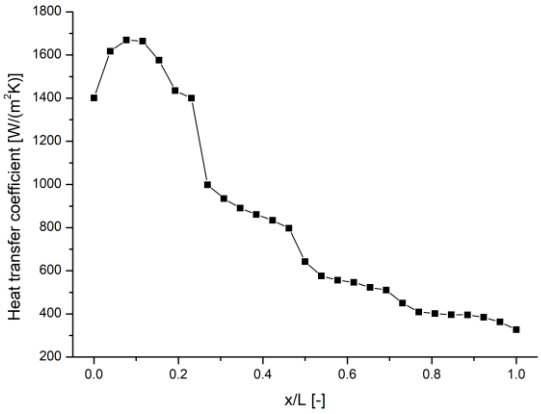

Figure 16. HTC distributions for the stator surface (Pressure ratio = 1.6, N = 4703 rpm, s = 1.2 mm)

The thermal-fluid-structural model was developed to provide insights into the extent to which the low-pressure turbine stator well represented an adiabatic system, the effect of heat convection on the leakage performance and total temperature rise, and the importance of choosing correct boundary conditions that describe the real turbine seal operation.

The total temperature rise was calculated utilizing the iterative computation approach described in Section 4.2. In contrast to the CFD-Adiabatic calculation, Figure 17 shows the increase in total temperature with different pressure ratios when using the thermal-fluid-structural model, which accounts for the impacts of windage heating and heat transfer together. The effect of heat transfer is greater while the rise in seal output total temperature is more obvious with fewer pressure differences. Figure 18 depicts the total heat generation comparison between CFD-Adiabatic calculation and thermal-fluid-structural model, the numerical difference ranges from 1 kw to 3.5 kw, and the heat generation difference decreases with increasing pressure ratio.

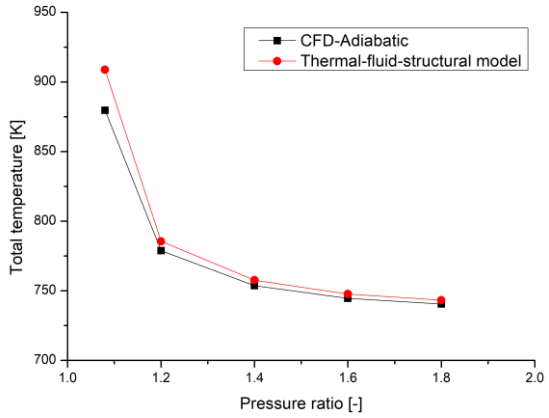

Figure 17. Changes in total temperature at the labyrinth seals outlet for varying seal pressure ratios

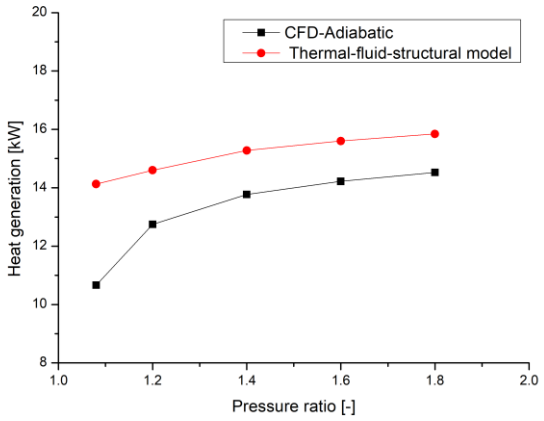

Figure 18. Heat generation by the seal cavity for varying seal pressure ratios

6. Conclusions

Throughout the research investigation, several conclusions were drawn about the flow and thermal characteristics of the typical low-pressure turbine well. Further analysis using the thermal-fluid-structural model allowed for a deeper exploration of the importance of using the correct boundary conditions in simulation and confirmed that the heat convection flux should not be ignored compared with the adiabatic condition. With an adiabatic system in computational simulations, the method of using windage heating, based on an adiabatic system, to characterize the leakage and thermal performance in the turbine stator well was not entirely adequate. Thus, using a combination of a one-dimensional axisymmetric heat transfer model and a thermal-fluid-structural calculation process, numerical methods for obtaining heat transfer coefficients across rotor and stator were developed and applied to the labyrinth seal region in the turbine stator well with consideration of heat convection and windage heating. The computational and turbulence models, as well as mesh density, are all thoroughly analyzed and explained in depth in order to verify the proposed method.

The thermal-fluid-structural model was developed to provide insights into the extent to which the low-pressure turbine stator well represented an adiabatic system, the influence of convection on the leakage and thermal performance of a narrow flow path at different seal pressure ratios, and the significance of selecting the correct boundary conditions that describe the real seal operation. For varied seal pressure ratios ranging from 1.08 to 1.8, a 3D axisymmetric CFD model of a straight-type labyrinth seal in the turbine stator well is utilized to examine leakage flow rate, windage heating, and heat convection.

First, a heat convection thermal boundary condition was implemented into the model and compared to the adiabatic boundary condition. The results indicated that with increasing pressure difference, total temperature rise across the seal reduced, and the adiabatic condition underestimated the labyrinth seal's outlet temperature and total heat generation for a constant seal pressure ratio. This prompted the implementation of a thermal model that was developed using the converged wall temperatures from the one-dimensional axisymmetric heat transfer model. Thus, for a good low-pressure turbine stator well design, precise characterization of the heat transfer coefficient, windage heating, and leakage flow rates was essential.

Acknowledgment

This work was supported by funding from the National Science and Technology Major Project (J2019-IV-0010-0078). Authors acknowledge the support of China Scholarship Council and Faculty of Aerospace Engineering, Northwestern Polytechnical University.

References

[1] M. Micio, B. Facchini, L. Innocenti, F. Simonetti, Experimental Investigation on Leakage Loss and Heat Transfer in a Straight Through Labyrinth Seal, Volume 5: Heat Transfer, Parts a and B. (2011).

[2] K. He, J. Li, X. Yan, Z. Feng, Investigations of the conjugate heat transfer and windage effect in stepped labyrinth seals, International Journal of Heat and Mass Transfer. 55 (2012) 4536–4547.

[3] K. Charan Nayak, P. Dutta, Effect of Rub-Grooves on Leakage and Windage Heating in Straight-Through Labyrinth Seals, Journal of Tribology. 138 (2015).

[4] X. Kong, G. Liu, Y. Liu, L. Zheng, Experimental testing for the influences of rotation and tip clearance on the labyrinth seal in a compressor stator well, Aerospace Science and Technology. 71 (2017) 556–567.

[5] M. Flouros, F. Cottier, M. Hirschmann, C. Salpingidou, Numerical Investigation on Windback Seals Used in Aero Engines, Aerospace. 5 (2018) 12.

[6] E. Campagnoli, A. Desando, Validation of a CFD Model of a Labyrinth Seal for Low Pressure Turbines Using a Fluid-Thermal Tool Tuned Through Experimental Measurements, Instrumentation Mesure Métrologie. 18 (2019) 509–516.

[7] D. Sun, M. Zhou, H. Zhao, J. Lu, C.-W. Fei, H. Li, Numerical and Experimental Investigations on Windage Heating Effect of Labyrinth Seals, Journal of Aerospace Engineering. 33 (2020) 04020057.

[8] K.C. Nayak, Effect of Rotation on Leakage and Windage Heating in Labyrinth Seals With Honeycomb Lands, Journal of Engineering for Gas Turbines and Power. 142 (2020).

[9] Z. Wang, B. Zhnag, Y. Chen, S. Yang, H. Liu, H. Ji, Investigation of Leakage and Heat Transfer Properties of the Labyrinth Seal on Various Rotation Speed and Geometric Parameters, Coatings. 12 (2022) 586–586.

[10] Y. Shi, S. Ding, T. Qiu, P. Liu, C. Liu, Nonuniform Clearance Effects on Windage Heating and Swirl Development in Straight-Through Labyrinth Seals, Journal of Aerospace Engineering. 35 (2022).

[11] B. Zhang, S. Yang, J. Zhang, Z. Lin, H. Ji, Experimental investigation on relationship between heat transfer and sealing characteristics under different pressure ratios in labyrinth seals with orthogonal method, Ain Shams Engineering Journal. 14 (2023) 101990.

[12] S. Yang, W. Du, L. Luo, S. Wang, B. Sunden, The sealing capacity and heat transfer characteristics of a straight-through labyrinth seal with different geometric parameters, Heat Transfer Research. 54 (2023) 53–73.

[13] P. Sun, C. Liu, Quantifying the impact of heat in support seal configuration for aero engines, The Aeronautical Journal. 127 (2023) 1698–1716.

[14] Y. Shi, S. Ding, P. Liu, T. Qiu, C. Liu, C. Qiu, D. Ye, Swirl Flow and Heat Transfer in a Rotor-Stator Cavity with Consideration of the Inlet Seal Thermal Deformation Effect, Aerospace. 10 (2023) 134.

[15] R. Jackson, L. Christodoulou, Z. Li, C.M. Sangan, S.E. Ambrose, R. Jefferson-Loveday, G. Lock, J.A. Scobie, Influence of swirl and ingress on windage losses in a low-pressure turbine stator-well cavity, Experiments in Fluids. 64 (2023).

[16] Z. Liu, P. Jiang et al. Mechanical system design of aviation gas turbine engine. China Science Publishing & Media Ltd., 2022.

[17] J.A. Millward, M.F. Edwards, Windage Heating of Air Passing Through Labyrinth Seals, Journal of Turbomachinery. 118 (1996) 414–419.

Paper submitted: 23 January 2024
Paper revised: 13 June 2024
Paper accepted: 14 June 2024